ELSEVIER

Contents lists available at ScienceDirect

Solar Energy

journal homepage: www.elsevier.com/locate/solener



CdS barrier to minimize Zn loss during CdCl₂ treatment of Cd-Zn-Te absorbers



Tushar M. Shimpi^{a,*}, Drew E. Swanson^a, Jennifer Drayton^b, Ali Abbas^c, John M. Walls^c, Kurt L. Barth^a, Walajabad S. Sampath^a

- ^a Department of Mechanical Engineering, Colorado State University, Fort Collins, CO 80523, USA
- ^b Physics Department, Colorado State University, Fort Collins, CO 80523, USA
- ^c Center for Renewable Energy Systems Technology, Wolfson School of Mechanical, Electrical and Manufacturing Engineering, Loughborough University, Leicestershire LE11 3TU, UK

ARTICLE INFO

Keywords: High band gap II–VI solar cells Tandem solar cells Cadmium chloride treatment on Cd-Zn-Te and Co-sublimation of Cd-Zn-Te CdTe alloys Top cell in multi-junction solar cell

ABSTRACT

A major challenge in the fabrication of high band gap II–VI polycrystalline solar cells is to preserve the original composition of the absorber after the CdCl₂ activation treatment. In this study, a method is demonstrated to maintain the Cd-Zn-Te alloy absorber composition during its exposure to the CdCl₂ treatment. A thin film of CdS was applied as a barrier on the back surface of the high band gap polycrystalline $Cd_{(1-x)}Zn_xTe$ (x=20% by atomic ratio, corresponding band gap $1.72\,eV$) before the CdCl₂ treatment. Using transmission electron microscopy and energy dispersive spectroscopy, it was observed that the composition of Cd-Zn-Te was maintained after the CdCl₂ treatment. The devices fabricated after removing the thin film of CdS, exhibited diode-like behavior. A significant increase in the quantum efficiency near the short wavelength region was observed, and the band gap of $Cd_{(1-x)}Zn_xTe$ was maintained.

1. Introduction

CdCl₂ treatment is an essential step during the fabrication process of solar cells fabricated with CdTe-based materials and alloys. It is known that the CdCl₂ treatment of CdTe improves the device performance (Morales-Acevedo, 2006; Wu, 2004), enhances grain growth (Abbas et al., 2013; Kim and Sohn, 2016; McCandless et al., 1997; Munshi et al., 2016), decorates the grain boundaries of the CdTe grains with chlorine (Li et al., 2014) and removes stacking faults from the CdTe absorber layer (Abbas et al., 2013). In the CdCl2 treated devices with CdS as a window layer adjacent to the front contact, the chlorine was also visible in the grain boundaries of the CdS film and at the interface between the CdS and the CdTe (Abbas et al., 2013). Recently, an efficiency of over 21% has been reported for CdTe with a modified band gap by First Solar, Inc. (Best Research-Cell Efficiencies Chart, 2017) and device efficiencies may be further improved by stacking individual junctions in sequence of decreasing band gap to minimize thermalization losses (Brown and Wu, 2009).

Studies on tandem devices using CdTe and ternary alloys of CdTe for the top cell coupled with silicon or copper-indium-gallium-diselenide as bottom cells indicate that improvements in the efficiency (Coutts et al., 2003) and power generation costs are obtainable (Tamboli et al., 2017;

Devices fabricated from an as-deposited CdTe alloy on a selective window layer, such as a thin film of CdS, without any CdCl2 treatment display poor device performance (Martinez et al., 2015; Lee et al., 2004; Shimpi et al., 2016). Researchers have used the CdCl₂ activation treatment on CdTe alloys and the studies report limited success in retaining the original composition of the CdTe alloy (Martinez et al., 2015; Mccandless et al., 2006; Lee et al., 2005; Reich et al., 2016). A major hurdle in the fabrication of high band gap solar cells using CdTe alloys has been reducing the loss of the alloying elements from the ternary compound during the CdCl_2 treatment. This loss is due to formation of volatile chloride compounds such as $\rm ZnCl_2$, $\rm MgCl_2$ and $\rm MnCl_2$ (Lee et al., 2004; Shimpi et al., 2016; Dhere et al., 2003; McCandless et al., 2006) which then vaporize. Even though the performance of the device is generally improved after the CdCl₂ treatment, the residual film often has a lower band gap than the as-deposited film. This is seen through the shift in the band edge due to loss of one of the elements

E-mail address: mechanical.tushar@gmail.com (T.M. Shimpi).

Sofia et al., 2017). For two-junction solar cells, numerical calculations indicate a band gap of 1.72 eV is optimal for the top cell (Bremner et al., 2008) connected in series. The band gap of the ternary alloys of CdTe can be tuned by controlling the quantity of element X (Zn, Mg or Mn) in a $Cd_{(1-x)} X_x$ Te alloy (Martinez et al., 2015; Kobyakov et al., 2014; Dhere et al., 2003; Lee et al., 2004).

^{*} Corresponding author.

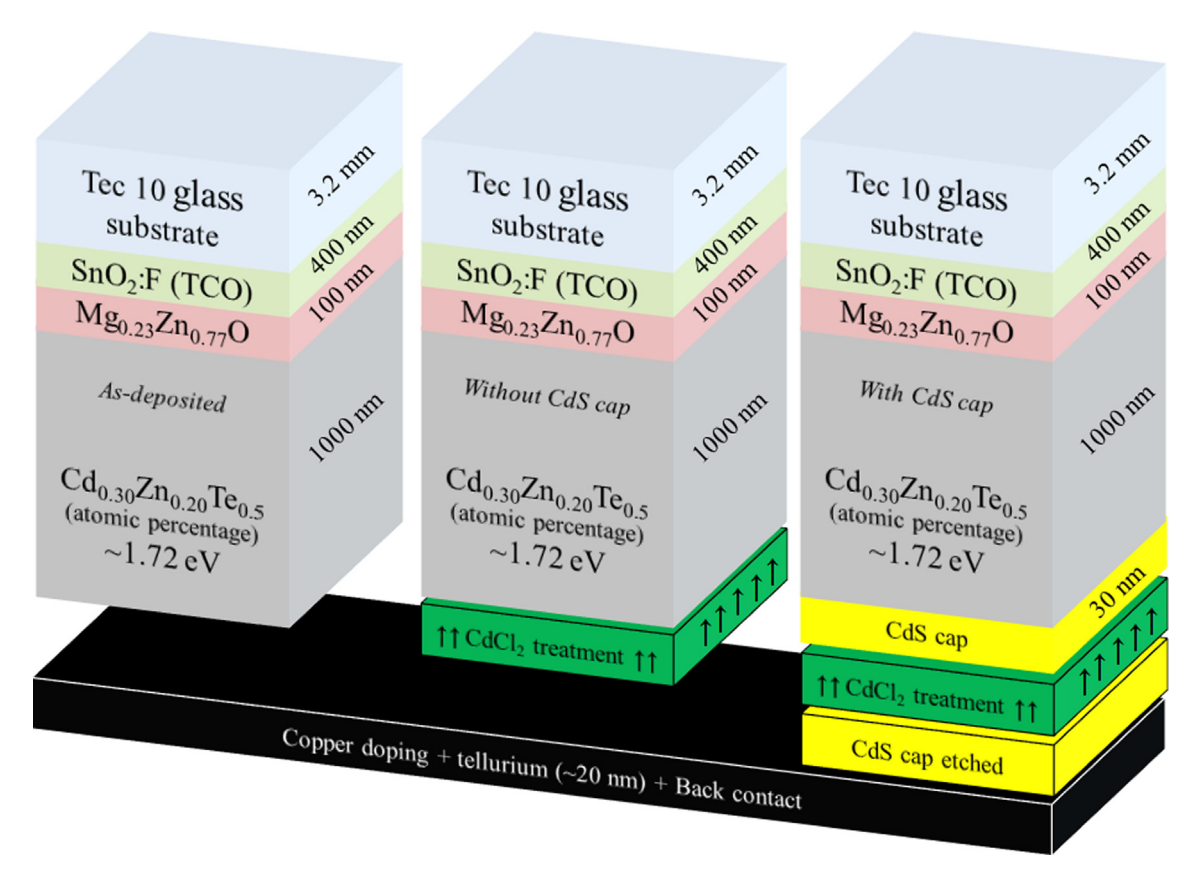


Fig. 1. Schematic of different Cd-Zn-Te device structures used during the CdCl₂ treatment.

(Zn, Mg and Mn) towards longer wavelength, and here the reduced band gap of the CdTe alloy is not optimized for a top cell.

In this study, the $Cd_{(1-x)}Zn_xTe$ (Cd-Zn-Te) alloy with a band gap of 1.72 \pm 0.02 eV was selected as an absorber for the high band gap solar cell. To maintain the composition of the absorber layer, a thin film of CdS referred to as a "CdS cap" was deposited on the Cd-Zn-Te film, and then a CdCl $_2$ treatment was carried out. Material characterization was performed with the CdS cap on the Cd-Zn-Te, and the solar cell was completed after etch removal of the CdS cap.

2. Experimental

The Cd-Zn-Te device structures used in the experiment are shown in Fig. 1.

Tec 10 glass substrates (NSG-Pilkington, Inc.) coated with a fluorine-doped tin-oxide transparent conducting oxide (TCO) on one side were ultrasonically cleaned prior to the deposition process. A thin buffer film of $\rm Mg_{0.23}Zn_{0.77}O$ (Mg-Zn-O) was sputter-deposited at room temperature using radio-frequency power from a single-alloy target onto the TCO (Kephart et al., 2016). The radio-frequency forward power used during sputtering was 1.70 W/cm² and the measured thickness of Mg-Zn-O was 100 nm.

The Cd-Zn-Te was deposited by co-sublimation (Kobyakov et al., 2014) of CdTe and elemental Zn. The co-sublimation hardware enables the flux of each material to be independently controlled. The band gap and thickness of the Cd-Zn-Te was calibrated by adjusting the source temperatures of CdTe and Zn to vary the alloy composition. The Cd-Zn-Te absorber layer was $\sim 1~\mu m$ thick with a band gap of 1.72 $\pm~0.02~eV$. Based on the database from the international center for diffraction data on X- ray diffraction, the approximate composition of the Cd-Zn-Te was estimated to be 20% by atomic ratio (Soliman et al., 1996). In a separate study, CdS deposition parameters were determined. After a vacuum break, the substrate with structure Mg-Zn-O/Cd-Zn-Te was reheated to

480 °C before the CdS film deposition in separate chamber. Initially, CdS films with different thicknesses were deposited on Tec10 glass samples, while the CdS source temperature, the Tec10 glass sample temperature and the process conditions were kept constant. Only the deposition time was varied. A non-uniform coverage was observed on the Tec10 glass with CdS film thickness less than 20 nm. The film thickness uniformity improved as the thickness increased. Considering that the thicker CdS cap on the CdZnTe would take longer to etch the CdS from CdZnTe, a film thickness of 30 nm for the CdS as a cap was deposited via sublimation on the back of the Cd-Zn-Te without breaking the vacuum (Swanson et al., 2016).

The CdCl₂ treatment was performed after the CdS cap deposition without breaking vacuum. The substrate temperature of the Mg-Zn-O/ Cd-Zn-Te/CdS entering the CdCl₂ station was 400 °C. The CdCl₂ station consisted of a graphite crucible loaded with CdCl2 beads and a graphite block above it. The substrate was inserted in between the graphite crucible and the graphite block. The graphite crucible and the graphite block were pre-heated separately and maintained at 437 °C and 386 °C (Swanson et al., 2016). The substrate was exposed to the CdCl₂ for 20 s (Kephart et al., 2016). After the CdCl₂ treatment, the substrate was transferred to an anneal station and maintained at 400 °C for 120 s. The substrate was then cooled to room temperature before rinsing the excess CdCl2 from the back surface using deionized water. The substrate was then dried using nitrogen. The plain Tec10 glass used as a witness coupon placed along with the substrate had 30 nm of CdS. The CdS on the back of Cd-Zn-Te was etched using 50% concentrated HCl acid solution and rinsed twice with deionized water to remove the residual HCl. The substrate then underwent a standard copper doping process (Swanson et al., 2016) followed by the deposition of a 20 nm thick Te layer evaporated on the back.

For the back electrode, films of carbon and nickel in acrylic binders were applied using a spray technique. Small area devices were delineated by abrasive blasting and an indium ring was soldered to the TCO

to form the front contact (Swanson et al., 2016). To understand the effectiveness of using a CdS cap acting as a barrier during the $CdCl_2$ treatment, two control samples were fabricated with the same deposition process. On one control sample, the $CdCl_2$ treatment was carried out on samples processed similarly but without a CdS cap. On the other control sample, devices were fabricated with as-deposited Cd-Zn-Te (no $CdCl_2$ treatment). The copper doping process, application of back electrode and small area delineation processes were the same for both control samples.

The band gap of the Cd-Zn-Te film was determined by using Tauc plots based on the optical transmission measurements. For transmission, the wavelength was scanned from 350 nm to 900 nm with a dualbeam spectrometer from Ocean Optics Inc. The device performance was evaluated by current density vs voltage (J-V) plots and external quantum efficiency (EQE) measurements. The J-V testing was carried out under AM 1.5 illumination in a Solar Light Co. solar simulator at room temperature. For EQE, the wavelength was swept from 350 nm to 900 nm under zero bias conditions. For material composition analysis, a device cross section with the CdS cap was prepared for transmission electron microscopy and EDS elemental mapping to investigate the residual composition of the alloy after the CdCl2 treatment. The cross section was fabricated by using an in-situ lift off process on a FEI Nova 600 Nanolab dual beam system and was mounted on to a copper grid. For viewing the specimen, a FEI Tecnai F20 Transmission Electron Microscope (TEM) equipped with an Oxford Instruments EDX detector was used. Line scans for composition profiling were performed and analyzed using AZtec software. The Glancing Angle X-Ray Diffraction (GAXRD) was performed using a Bruker D8 system. The X-rays were generated using a copper source with K_{alpha1} radiation of 1.54046 Å. The diffraction patterns were fitted with Split-Pearson7 function to determine the peak locations, which were then compared to the standard cards from the database provided by International Center for Diffraction Data (ICDD).

3. Results and discussions

3.1. Optical transmission

Transmission measurements were taken at different stages of the fabrication process (Fig. 2). The band gap of the as-deposited Cd-Zn-Te calculated from a Tauc plot was $1.72\pm0.02\,\mathrm{eV}$. After the CdCl₂ treatment on Cd-Zn-Te without the CdS cap, the band gap shift towards the longer wavelength region was observed. The shift in the band gap occurred due to the loss of zinc in the form of ZnCl₂ during the CdCl₂

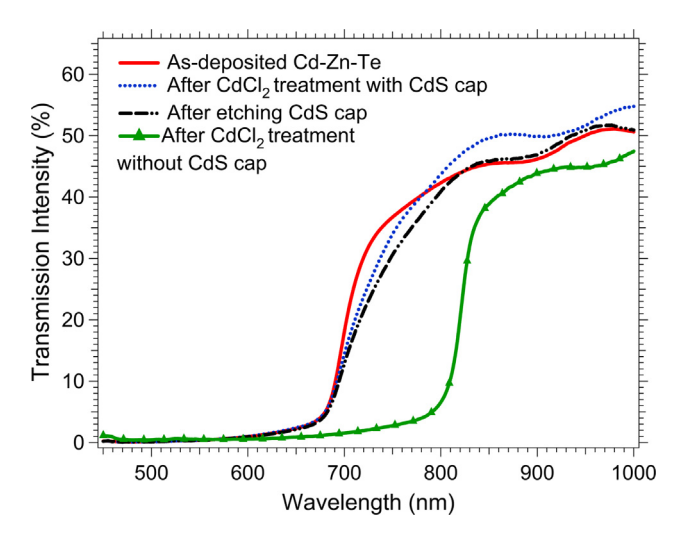


Fig. 2. Transmission measurements on Cd-Zn-Te samples at different stages of fabrication.

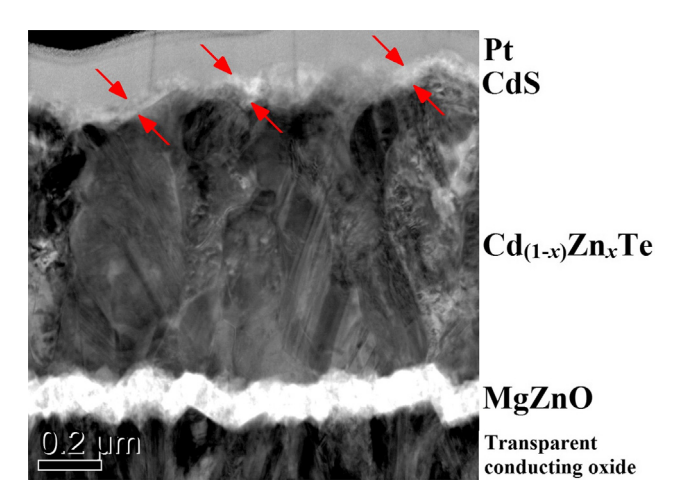


Fig. 3. Bright field TEM image of the cross-section of the specimen prepared before etching thin film of CdS cap.

treatment (Dhere et al., 2003; Shimpi et al., 2016; Mccandless et al., 2006; Lee et al., 2004). The CdS band gap calculated during the calibration process was 2.4 eV. When CdS was deposited on the Cd-Zn-Te, no shift in its band edge was observed. After the CdCl $_2$ treatment and removal of the CdS by HCl solution, the band gap of the Cd-Zn-Te absorber was measured at 1.70 eV. This minor reduction was taken as a good indication that there was little or no formation of CdTe in the Cd-Zn-Te film and that the majority of the zinc was retained in the Cd-Zn-Te after the CdCl $_2$ treatment.

3.2. Transmission electron microscopy

A cross sectional bright field TEM image of the device prepared from the Mg-Zn-O/Cd-Zn-Te/CdS cap structure following treatment with CdCl₂ is shown in Fig. 3. The arrows in Fig. 3 indicate position of the CdS cap on Cd-Zn-Te. The coverage of the CdS film on the Cd-Zn-Te appears to be conformal and uniform. The Cd-Zn-Te film was polycrystalline and void free after the CdCl₂ treatment. The as-deposited Cd-Zn-Te grains from the co-sublimation process are columnar (Swanson et al., 2018). After the CdCl₂ treatment, the morphology of the grains changed to a more granular shape. This indicated that the recrystallization had occurred without an increase in grain size. The stacking faults within the individual grains were absent, consistent with observations reported for CdTe films treated with CdCl₂ at high temperatures (Munshi et al., 2018).

The elemental maps obtained from the EDS detector are displayed in Fig. 4 and the individual maps are labeled with the respective element. The concentration of zinc was retained in the bulk of Cd-Zn-Te film after the CdCl2 treatment though a slight loss of zinc in the form of ZnCl₂ (McCandless et al., 2006) may have occurred near the surface of Cd-Zn-Te through the CdS film. Similar small reductions at the back surface were observed when a lower temperature CdCl₂ treatment was performed on the sputtered Cd-Zn-Te and co-sublimated Cd-Zn-Te with a CdTe cap (Swanson et al., 2018). Chlorine was observed to segregate along the grain boundaries of the Cd-Zn-Te film and accumulation of chlorine was also observed along the Cd-Zn-Te/Mg-Zn-O interface. The presence of chlorine in the grain boundaries of Cd-Zn-Te without causing a loss of zinc is significant, since this is the first such observation reported. The presence of chlorine along the grain boundaries has been previously identified as beneficial in devices with CdTe absorbers (Munshi et al., 2018).

In the tellurium composition map, the signal obtained was uniform which indicates that no other phases are formed after the $CdCl_2$ treatment. The cadmium signal was brighter in the areas where zinc loss had occurred and in the CdS film. The oxygen was detected in the Mg-Zn-O film, and any oxide formation in the bulk of Cd-Zn-Te was below the

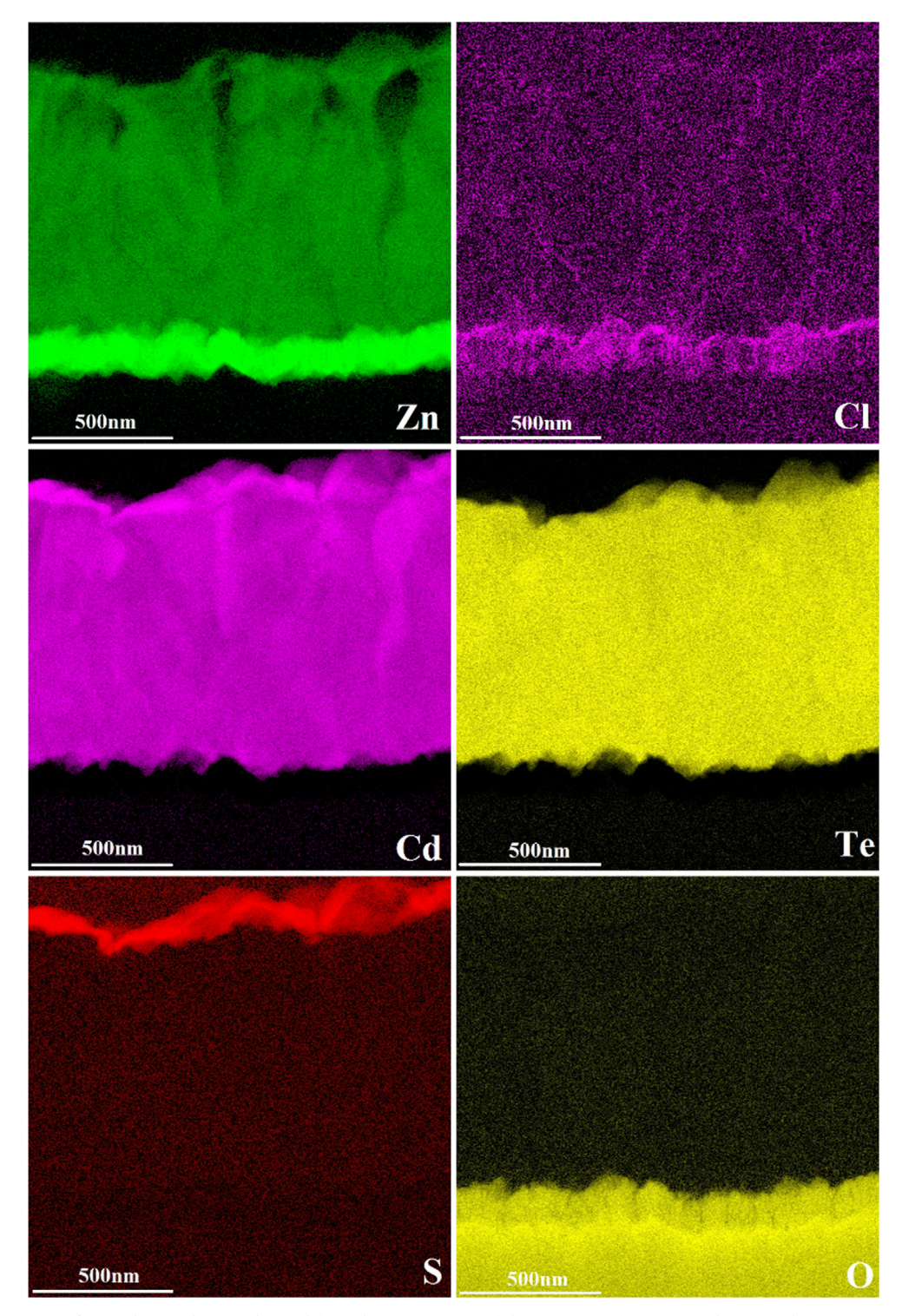
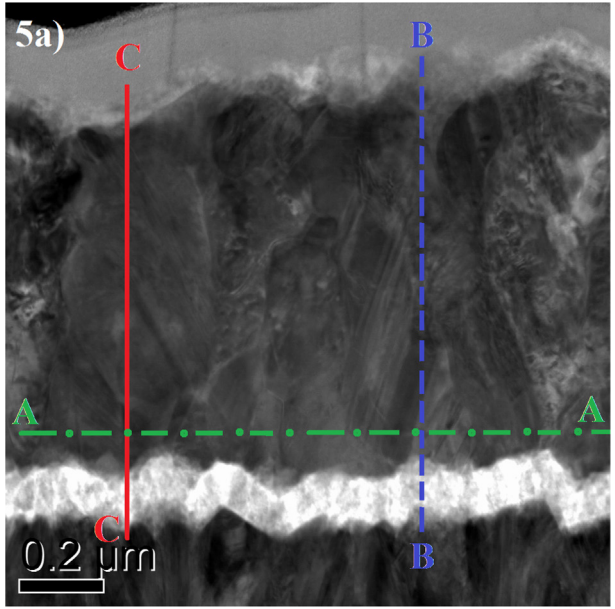


Fig. 4. Elemental maps obtained from the cross section of the specimen of Mg-Zn-O/Cd-Zn-Te/CdS cap.

detection limit. The Mg-Zn-O buffer was unchanged with the CdCl_2 treatment and no diffusion of magnesium or excess zinc in the bulk of Cd-Zn-Te was observed.

To quantitatively determine the composition of Cd-Zn-Te film, EDS line scans were performed at different locations on the device cross-section. The positions of the line scans and composition profile for each line are shown in Fig. 5(a)–(d). The overall composition measured for different line scans is summarized in Table 1. The contributions from the elements O, Cl and Mg in the bulk of Cd-Zn-Te were small and are not included.

In the line scan A-A parallel with the interface, there was no discernible variation in the zinc concentration. The average composition calculated (1.68 eV) was close to that of the as-deposited Cd-Zn-Te film. Small amounts of chlorine were observed along the grain boundaries of Cd-Zn-Te and also at the interface of Mg-Zn-O/Cd-Zn-Te. In the CdCl₂ treatment on CdTe, chlorine decorates the CdTe grain boundaries and improves the efficiency of the CdTe devices by reducing the defects in the absorber (Morales-Acevedo, 2006; Wu, 2004; Abbas et al., 2013; Kim and Sohn, 2016; McCandless et al., 1997; Munshi et al., 2016). So based on the observations on CdTe treated with CdCl₂, the presence of



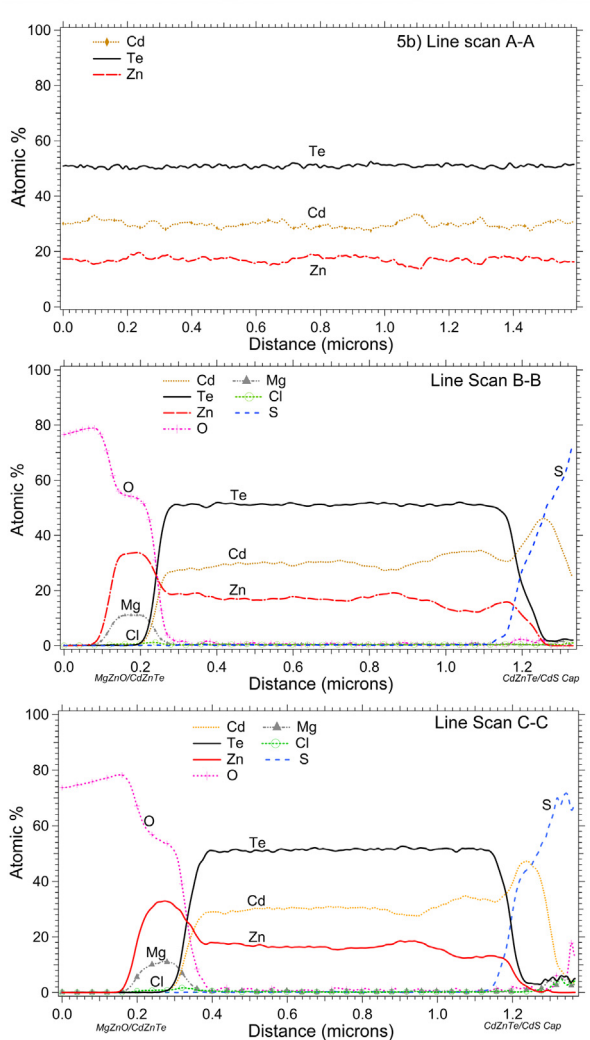


Fig. 5. Line scans conducted on the cross-section of the specimen. (a) Locations of the line scans on the cross-section of the specimen. (b)–(d) are the composition profiles generated by different line scans.

chlorine suggests that the Cd-Zn-Te absorber quality has improved by passivation of grain boundaries and by removing some of the defects from the as-deposited material. The retention of the original concentration of Zn after the $CdCl_2$ treatment combined with the presence of chlorine along the grain boundaries from the EDS maps is a significant result.

The cross-section line scans B-B and C-C are divided into two regions for analysis. The first region is from the Mg-Zn-O/Cd-Zn-Te interface to approximately half way into the bulk of the Cd-Zn-Te, and the second region is that close to the Cd-Zn-Te/CdS interface. On both vertical line scans, the regions close to the Mg-Zn-O/Cd-Zn-Te interface have the same Cd-Zn-Te composition as the as-deposited Cd-Zn-Te. Near the region close to Cd-Zn-Te/CdS interface, a small loss of zinc is observed. The loss of zinc from Cd-Zn-Te may have occurred due to the formation of volatile ZnCl₂ compound during the CdCl₂ treatment and also due to the diffusion of zinc into the CdS forming Cd_(1-x)Zn_xS.

3.3. GAXRD

In previous studies, zinc loss has been reported to initiate at the back surface of Cd-Zn-Te and then progress towards the bulk during the CdCl₂ treatment (Shimpi et al., 2016). To examine the current samples, an X-ray at glancing angle of 3° was selected to probe the Cd-Zn-Te film surface and minimize the diffracted signal from the underlying TCO film. In addition, the diffraction pattern from bare Tec10 glass sample was used to compare the TCO peaks generated from the Cd-Zn-Te samples. The diffraction patterns generated are shown in Fig. 6.

In the as-deposited Cd-Zn-Te sample, the diffracted peaks (24.32°, 40.26°, 47.62°) match closely with the alloy composition of $Cd_{0.3}Zn_{0.2}Te_{0.5}$ by atomic percentage (ICDD card #00-015-1439). The peaks from other compositions of Cd-Zn-Te were not visible, indicating a single phase Cd-Zn-Te alloy was deposited through the co-sublimation process. Based on the intensity of the peaks, the preferred orientation of the Cd-Zn-Te film was along {1 1 1} plane corresponding to the peak at 24.32°. The GAXRD peaks also shifted towards a lower angle in the sample that had gone through the CdCl $_2$ treatment and without any CdS cap. The peaks at 23.74°, 39.28° and 46.4° corresponded to CdTe peaks (ICDD# 00-015-0770). The peaks from Cd-Zn-Te alloy were absent suggesting a complete loss of zinc from Cd-Zn-Te during the CdCl $_2$ treatment.

The sample fitted with the CdS cap during the CdCl $_2$ treatment showed minor changes in the Cd-Zn-Te alloy composition. The three peaks in this case (24.36°, 40.44° and 47.68°) corresponded closely to the as-deposited Cd-Zn-Te composition. New peaks, however were identified at 23.86°, 39.5° and 46.64° locations. Using the peak location at 23.86° and Vegard's equation (Ringel et al., 1989) for Cd-Zn-Te, the composition of the alloy formed was $Cd_{0.45}Zn_{0.05}Te_{0.5}$ by atomic percentage. From the optical transmission measurements and EDS maps, there was no shift in the band edge and loss of zinc initiated from the back surface of Cd-Zn-Te absorber. These observations indicate that the formation of $Cd_{0.45}Zn_{0.05}Te_{0.5}$ alloy is in low concentrations and near the back surface of Cd-Zn-Te absorber. In both the samples treated with the CdCl $_2$, the intensities of the peaks did not change significantly. The preferred orientation along {1 1 1} plane remained the same.

3.4. Device performance

The J-V performance of the devices is shown in Fig. 7. The voltage was scanned from $-0.8\,V$ to $1.2\,V$ under AM1.5 illumination. The J-V plot obtained from the as-deposited Cd-Zn-Te (no CdCl $_2$ treatment) varies linearly with respect to voltage and behaves as a resistor. The dark J-V is flat and indicates that the as-deposited Cd-Zn-Te does not form a good diode under zero illumination conditions. The device fabricated from the control sample that had undergone the CdCl $_2$ treatment without CdS cap also showed diode like behavior in the J-V plots.

Table 1
Composition of Cd-Zn-Te obtained from different line scans.

Fig. 5	Line scan	Distance (µm)	Atomic %					
			Cd	Zn	Te	S	$Cd_{(1-x)}Zn_xTe$	Estimated bang gap of $Cd_{(1-x)}Zn_xTe$ (eV)
(a) and (b)	A-A	0–1.5	29.87	17.14	50.85	_	Cd _{29.87} Zn _{17.14} Te	1.68
		std. dev.	1.86	1.53	1.73	-		
(a) and (c)	В-В	0.3-0.8	29.50	17.23	51.16	_	${\rm Cd}_{29.50}{\rm Zn}_{17.23}{\rm Te}$	1.68
		std. dev.	1.41	1.12	1.33	-Below 0.3		
		0.9-1.1	32.59	14.28	51.17	_	Cd _{32.59} Zn _{14.28} Te	1.63
		std. dev.	2.06	2.00	1.33	Below 0.3		
(a) and (d)	c-c	0.44-0.84	30.26	~17.00	51.32	Below 0.2	$Cd_{30.26}Zn_{17.00}Te$	1.68
		std. dev.	0.97	0.8	1.09	_		
		1.0-1.1	33.33	13.49	51.62	-Below 0.2	Cd _{33.33} Zn _{13.49} Te	1.62
		std. dev.	1.39	1.26	1.13	_		
		1.1-1.3	37.97	7.24	24.90	27.06	In the CdS cap	-
		std. dev.	6.34	5.46	20.81	21.56		

Standard deviation (std. dev.).

The conversion efficiency of the device fitted with a CdS cap during the CdCl₂ treatment was ~3.3% with a short circuit current density equal to 12.5 mA/cm². Theoretically, an absorber with a 1.72 eV band gap and no optical losses should produce ~21 mA/cm² of current density. If the estimated optical losses (Topič et al., 2015) from glass absorption (3 mA/cm²), reflection (1 mA/cm²) and back contact (1 mA/ cm²) are taken into consideration, the measured Jsc corresponds to approximately 75% of the available incident light, at zero bias and larger amount in reverse bias. The dark J-V plot exhibited a diode like behavior with a low series resistance at the back. There is a cross over between the dark and light J-V plot which may imply that that there is some recombination or a barrier at the Mg-Zn-O/Cd-Zn-Te interface. The measured open circuit voltage was under 600 mV and the fill factor measured was ~45%. One of the ways open circuit voltage and fill factor may be improved is by pairing with a more compatible n-type window layer (Liyanage et al., 2018). There was no roll over observed in the light or the dark J-V measurements which is a good indication that no residual CdS remained at the back of Cd-Zn-Te acting as a back barrier. Its performance was higher than the device without a CdS cap during the CdCl2 treatment.

In the EQE measurements (Fig. 8), the as-deposited control device, the light absorption was poor but the band edge was maintained. The

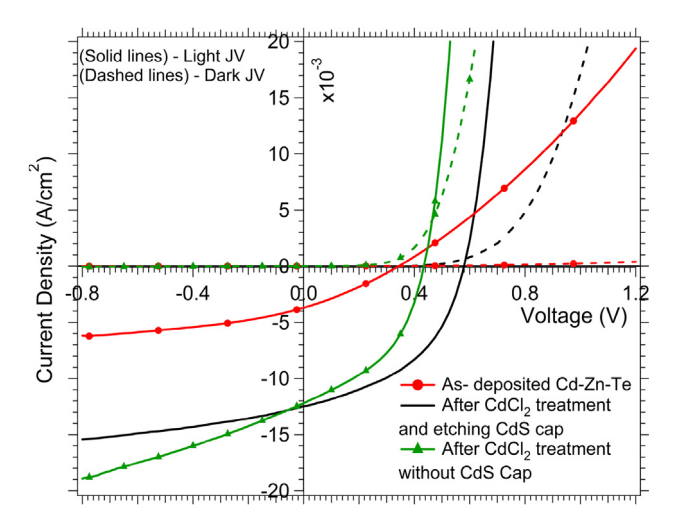
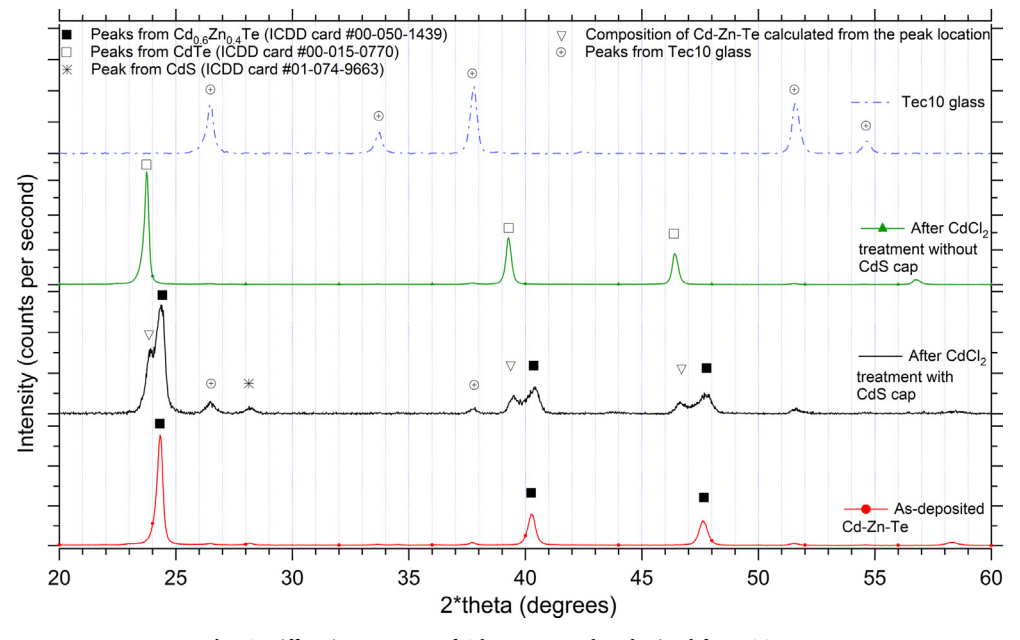


Fig. 7. Current density vs voltage plots.



 $\textbf{Fig. 6.} \ \ \textbf{Diffraction patterns of Cd-Zn-Te samples obtained from GAXRD}.$

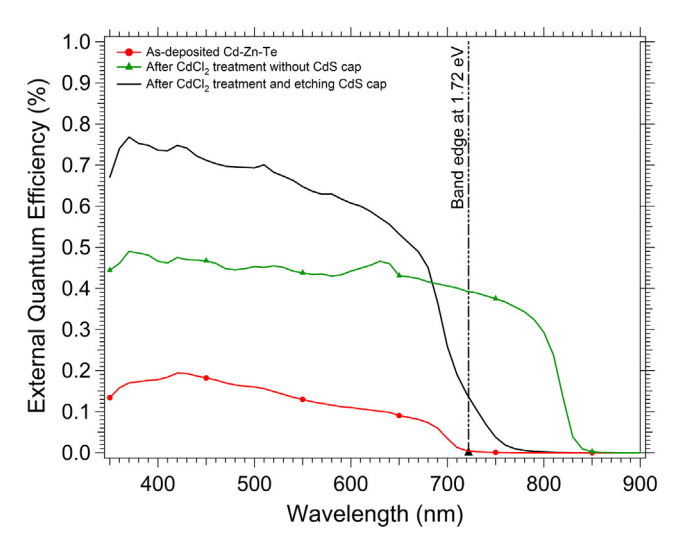


Fig. 8. External quantum efficiency plot on the device fabricated with Mg-Zn-O/Cd-Zn-Te.

current generation was observed from the longer wavelength region in the device fabricated after the $CdCl_2$ treatment without a CdS cap. The band gap in this case was shifted to ~ 1.5 eV, i.e close to CdTe band gap. The shift in the band gap towards the longer wavelength implies that without the CdS cap, the zinc from the as-deposited Cd-Zn-Te was lost and the composition of Cd-Zn-Te had changed to a lower band gap material (CdTe), which would be no longer suitable for the top cell in a two-junction tandem solar cell.

The signal obtained from the device with a CdS cap during the CdCl $_2$ treatment showed good light absorption by the Cd-Zn-Te absorber layer in the shorter wavelength regions. Consistent with a 1.72 eV band gap, there was no signal generated beyond 750 nm. The EQE plot combined with the transmission results, therefore indicate that the Cd-Zn-Te alloy composition was largely maintained after the CdCl $_2$ treatment. The absolute value of the first derivative of the EQE curve shown as a dashed line indicates that the average band gap of the material is at $\sim 1.74\,\mathrm{eV}$ corresponding to 700 nm. The current collected under zero bias was calculated by integrating the area under the EQE curve and was $12.9\,\mathrm{mA/cm}^2$.

4. Conclusions and future work

In this paper, we have demonstrated a method for preserving the zinc in Cd-Zn-Te solar-cell absorber after they are subjected to the CdCl₂ treatment. The CdS cap acted as a barrier for zinc to escape during the CdCl₂ treatment. No significant change in the band gap of Cd-Zn-Te was observed after the CdCl₂ treatment through most of the device. Modest zinc loss, however, was detected near the back of Cd-Zn-Te in the optical transmission, GAXRD measurements and from the elemental maps obtained from EDS. The Cl signal was preferentially, observed along the grain boundaries of Cd-Zn-Te and at the interface of Mg-Zn-O/Cd-Zn-Te. The Cd-Zn-Te did undergo recrystallization after the CdCl₂ treatment. The quantum efficiency, displayed good absorption at shorter wavelengths and the band edge was maintained at or near the original 1.72 eV.

The device fabricated from the as-deposited Cd-Zn-Te did not exhibit a rectifying curve and confirmed that the CdCl₂ treatment is essential for the alloy as well as for CdTe. The device fabricated with the CdCl₂ treatment without a CdS cap showed significant loss of zinc. The composition of Cd-Zn-Te changed to that of a lower band gap material, essentially becoming a CdTe absorber.

In this method, the deposition of the CdS cap and removal after the $CdCl_2$ treatment is a simple and straight forward process. In future work, this method should also be useful for other ternary alloys of CdTe

such as Cd-Mg-Te and Cd-Mn-Te to prevent changes in composition during the CdCl_2 treatment.

Acknowledgements

The co-sublimation and device fabrication work at Colorado State University was funded by Nation Science Foundation: Accelerating Innovation Research and Industry/University Cooperative Research Centers programs. The specimen preparation and TEM/EDS analysis at Loughborough University was supported by Engineering and Physical Science Research Council - Supergen SuperSolar Hub. The authors are grateful to the funding agencies. The authors are also grateful to Dr. James R. Sites for reviewing and suggesting changes in the manuscript body and the title. The maintenance of co-sublimation deposition chamber was regularly conducted by Carey Reich and authors are thankful to him. The high purity CdTe powder was purchased from 5N Plus, Inc. The interactions and suggestions from Dr. Jean-Nicolas Beaudry, 5N Plus, Inc. (Jean-Nicolas.Beaudry@5nplus.com), were very helpful and the authors are grateful to him. Authors would like to thank Anna Wojtowicz for performing the quantum efficiency measurement at PV lab, Department of Physics, Colorado StateUniversity. The authors are also thankful to the lab members of Next Generation PV, Department of Mechanical Engineering, Colorado State University for their support.

References

Abbas, A., Maniscalco, B., Bowers, J.W., Kaminski, P.M., West, G.D., Walls, J.M., 2013. Initiation of the cadmium chloride assisted re-crystallization process of magnetron sputtered thin film CdTe. In: Conf. Rec. IEEE Photovolt. Spec. Conf. pp. 1930–1934.

Abbas, A., West, G.D., Bowers, J.W., Isherwood, P., Kaminski, P.M., Maniscalco, B., Rowley, P., Walls, J.M., Barricklow, K., Sampath, W.S., Barth, K.L., 2013. The effect of cadmium chloride treatment on close-spaced sublimated cadmium telluride thinfilm solar cells. IEEE J. Photovolt. 3 (4), 1361–1366.

Best Research-Cell Efficiencies Chart, 2017. [Online]. Available: https://www.nrel.gov/pv/national-center-for-photovoltaics.html. (accessed: 10-Aug-2017).

Bremner, S.P., Levy, M.Y., Honsberg, C.B., 2008. Analysis of tandem solar cell efficiencies under AM1.5G spectrum using a rapid flux calculation method. Prog. Photovolt. Res. Appl. 16 (1), 225–233.

Brown, G.F., Wu, J., 2009. Third generation photovoltaics. Laser Photon. Rev. 3 (4), 394-405

Coutts, T.J., Ward, J.S., Young, D.L., Emery, K.A., Gessert, T.A., Noufi, R., 2003. Critical issues in the design of polycrystalline, thin-film tandem solar cells. Prog. Photovolt. Res. Appl. 11 (6), 359–375.

Dhere, R., Gessert, T., Zhou, J., Asher, S., Pankow, J., Moutinho, H., 2003. Investigation of CdZnTe for thin-film tandem solar cell applications. Mater. Res. Soc. Symp. – Proc. 763 (April), 409–414.

Dhere, R., Gessert, T., Zhou, J., Asher, S., Pankow, J., Moutinho, H., 2003. Investigation of CdZnTe for thin-film tandem solar cell applications. MRS Online Proc. Libr. Arch. 763 pp. null–null.

Kephart, J.M., Mccamy, J.W., Ma, Z., Ganjoo, A., Alamgir, F.M., Sampath, W.S., 2016.
Band alignment of front contact layers for high-efficiency CdTe solar cells. Sol.
Energy Mater. Sol. Cells 157, 266–275.

Kim, M.J., Sohn, S.H., 2016. In-situ HT-XRD study of CdTe thin-films during CdCl₂ heat treatment. Thin Solid Films 603, 272–275.

Kobyakov, P.S., Moore, A., Raguse, J.M., Swanson, D.E., Sampath, W.S., 2014. Deposition and characterization of $Cd_{1-x}Mg_xTe$ thin films grown by a novel cosublimation method. J. Vac. Sci. Technol. A Vac., Surf., Film. 32 (2), 021511.

Lee, S.H., Gupta, A., Compaan, A.D., 2004. Polycrystalline sputtered Cd(Zn, Mn)Te films for top cells in PV tandem structures. Phys. Status Solidi 1 (4), 1042–1045.

Lee, S.H., Gupta, A., Wang, S., Compaan, A.D., McCandless, B.E., 2005. Sputtered Cd₁xZn_xTe films for top junctions in tandem solar cells. Sol. Energy Mater. Sol. Cells 86

Li, C., Wu, Y., Poplawsky, J., Pennycook, T.J., Paudel, N., Yin, W., Haigh, S.J., Oxley, M.P., Lupini, A.R., Al-Jassim, M., Pennycook, S.J., Yan, Y., 2014. Grain-boundary-enhanced carrier collection in CdTe solar cells. Phys. Rev. Lett. 112 (15), 156103.

Liyanage, G.K., Phillips, A.B., Alfadhili, F.K., Heben, M.J., 2018. Numerical modelling of front contact alignment for high efficiency Cd_xZn_xTe and Cd_{1-x}Mg_xTe solar cells for tandem devices. MRS Adv. 2–6.

Martinez, O.S., Regalado-Pérez, E., Mathews, N.R., Morales, E.R., Reyes-Coronado, D., Galvez, G.H., Mathew, X., 2015. Photovoltaic performance of a $Cd_{1-x}Mg_xTe/CdS$ top-cell structure. Thin Solid Films 582 (May), 120–123.

McCandless, B.E., Moulton, L.V., Birkmire, R.W., 1997. Recrystallization and sulfur diffusion in CdCl₂-treated CdTe/CdS thin films. Prog. Photovoltaics Res. Appl. 5 (March), 249–260.

McCandless, B.E., Buchanan, W.A., Hanket, G.M., 2006. Thin film cadmium zinc telluride solar cells. In: IEEE 4th World Conference on Photovoltaic Energy Conference, pp.

483-486.

- Mccandless, B.E., Buchanan, W.A., Hanket, G.M., 2006. Thin film cadmium zinc telluride solar cells. pp. 483–486.
- Morales-Acevedo, A., 2006. Thin film CdS/CdTe solar cells: research perspectives. Sol. Energy 80 (6), 675–681.
- Munshi, A.H., Kephart, J.M., Abbas, A., Shimpi, T.M., Barth, K., Walls, J.M., Sampath, W.S., 2016. Effect of varying deposition and substrate temperature on sublimated CdTe thin-film photovoltaics. In: Conf. Rec. IEEE Photovolt. Spec. Conf. pp. 465–469.
- Munshi, A.H., Kephart, J.M., Abbas, A., Shimpi, T.M., Barth, K.L., Walls, J.M., Sampath, W.S., 2018. Polycrystalline CdTe photovoltaics with efficiency over 18% through improved absorber passivation and current collection. Sol. Energy Mater. Sol. Cells 176. 9–18
- Reich, C., Swanson, D., Shimpi, T., Drayton, J., Munshi, A., Abbas, A., 2016. Passivation of a Cd1-xMgxTe absorber for application in a tandem cell. pp. 487–491.
- Ringel, S.A., Sudharsanan, R., Rohatgi, A., Carter, W.B., 1989. A study of polycrystalline Cd (Zn, Mn) Te/CdS films and interfaces. J. Electron. Mater. 19 (3), 259–263.
- Shimpi, T.M., Kephart, J.M., Swanson, D.E., Munshi, A.H., Sampath, W.S., Abbas, A., Walls, J.M., 2016. The effect of the cadmium chloride treatment on RF sputtered Cd0.6Zn0.4Te films for application in multi-junction solar cells. J. Vac. Sci. Technol. A Vac., Surf., Film 1–16.

- Sofia, S.E., Mailoa, J., Weiss, D., Buonassisi, T., Peters, I.M., 2017. Cost analysis of tandem modules. 44th IEEE Photovoltaic Specialists Conference.
- Soliman, H.S., Allam, F.M., El-Shazly, Å.A., 2000. Structural and optical properties of $Cd_xZn_{(1:x)}Te$ thin films. J. Mater. Sci. Mater. Electron. 7 (1996), 233–239.
- Swanson, D.E., Kephart, J.M., Kobyakov, P.S., Walters, K., Cameron, K.C., Barth, K.L., Sampath, W.S., Drayton, J., Sites, J.R., 2016. Single vacuum chamber with multiple close space sublimation sources to fabricate CdTe solar cells. J. Vac. Sci. Technol. A Vac., Surf., Film. 34 (2), 021202.
- Swanson, D.E., Reich, C.R., Abbas, A., Shimpi, T.M., Liu, H., Ponce, F., Zhang, H., Metzger, W., Walls, J.M., Sampath, W.S., Holman, Z.C., 2018. CdCl₂ passivation of CdMgTe and CdZnTe absorbers for tandem photovoltaic cells. J. Appl. Phys. 123 pp. 203101 1–10.
- Tamboli, A.C., Bobela, D.C., Kanevce, A., Remo, T., Alberi, K., Woodhouse, M., 2017. Low-cost CdTe/silicon tandem solar cells. IEEE J. Photovolt. 7 (6), 1767–1772.
- Topič, M., Member, S., Geisthardt, R.M., Sites, J.R., 2015. Performance limits and status of single-junction solar cells with emphasis on CIGS. IEEE J. Photovolt. 5 (1), 360–365
- Wu, X., 2004. High-efficiency polycrystalline CdTe thin-film solar cells. Sol. Energy 77 (6), 803–814.